ELSEVIER

Solar Energy Materials & Solar Cells 73 (2002) 391–409

Solar Energy Materials & Solar Cells

www.elsevier.com/locate/solmat

Chemical stability of sputtered Mo/Sb_2Te_3 and Ni/Sb_2Te_3 layers in view of stable back contacts for CdTe/CdS thin film solar cells

Anke E. Abken*

Institut für Solarenergieforschung GmbH, D-30165 Hannover, Germany

Received 26 March 2001; received in revised form 20 December 2001

Abstract

Sb–Te phases sputtered from an $Sb_2Te_3/Sb/Te$ target in a substrate temperature range from 293 to 523 K are characterised by X-ray diffraction (XRD) and Hall measurements. A simple thermodynamic model is introduced for estimating the chemical stability of the Ni/Sb_2Te_3 and the Mo/Sb_2Te_3 interface. These data and the results of kinetic test reactions for sputtered Ni/Sb_2Te_3, Ni/Sb–Te, Mo/Sb_2Te_3 and Mo/Sb–Te layers are compared using XRD measurements. $Metal/Sb_2Te_3$ thin film double-layer systems are used as a model for an innovative back contact for CdTe/CdS thin film solar cells offering an improved long-term stability.

Keywords: $Sb2Te_3$; CdTe; CdS; Thin film solar cell; Back contact; Stability

1. Introduction

Metal-semiconductor contacts play an important role in device fabrication and long-term reliability and stability of CdTe based solar cells. One main problem of CdTe/CdS thin film solar cells is the formation of an ohmic contact [1]. The electron affinity of CdTe ($\chi = 4.5$ eV) is high so no metal or alloy which has a higher work function is available to avoid the formation of a Schottky contact. Doping of polycrystalline CdTe used in solar cells is limited by the strong tendency of self-compensation [2]. Nevertheless, the best strategy to overcome the contact problem is

*Corresponding author. Department of Physics, University of Durham, South Road, Durham DH1 3LE, UK. Tel.: +44-191-374-2395; fax: +44-191-374-7358.

E-mail address: anke.abken@gmx.net (A.E. Abken).

0927-0248/02/$ - see front matter
PII: S0927-0248(02)00207-6

to introduce a thin p^+-layer between the CdTe absorber and the metal back contact to form a tunnel contact [3]. The most common preparation technique to get a reliable contact is chemical etching [4–6] of the CdTe which leaves a Te-rich CdTe surface. Te-rich surface layers are susceptible to oxidation to TeO_2 [7]. Oxidation of Te or the CdTe itself leads to contact degradation by the formation of a metal/insulator/semiconductor (MIS) structure [8,9]. Niles et al. [10] show that etching to produce a Te-rich surface is more effective in minimising the Schottky barrier if etching is slightly prolonged. Perhaps this is accompanied by the penetration of metastable concentrations of excess Te (i.e. V_{Cd}) into the sub-surface region and may provide shunting. Chemical etching widens grain boundaries [11]. In this case, the back contact metal can diffuse easily along the grain boundaries, via V_{Cd} states and interstitials (M_i) through the bulk of the CdTe absorber. This might act to limit the long-term stability of the solar cell by contamination of the device with impurities originating from the back contact material. To avoid instability an alternative is to use a p^+-metal telluride intermediate layer with a high electron affinity which creates no barrier with CdTe. If thin, this intermediate telluride layer allows the formation of a tunnel contact. The intermediate layer may also act as a diffusion barrier for the contamination from the back contact metal. The electrical performance of the metal/intermediate telluride back contact system might be expected to depend on Fermi level pinning in the CdTe which itself is influenced by the processing history [3]. The low band gap Sb_2Te_3 ($E_{gap} = 0.3$ eV) satisfies these requirements most [12]. Metal/Sb_2Te_3/CdTe contacts were first used for CdTe solar cells by Romeo and co-workers in the form Mo/Sb_2Te_3/CdTe [12–16]. The stability of Sb_2Te_3/CdTe and Ni/Sb_2Te_3 systems has been investigated in Refs. [17,18].

Sputtering is a suitable technology that can be implemented in a low-cost fabrication process for CdTe/CdS solar cells and modules: it is also suitable for Sb_2Te_3 and metals [19]. However, in the development of Sb_2Te_3 for back contact applications, it is necessary to investigate the relationship of the materials quality to the sputtering conditions for the following reasons: Firstly, for the Sb_2Te_3 to be electrically continuous and to act as a reliable diffusion barrier the layer itself should be void and pin-hole free. Secondly, it is desirable to form the stoichiometric compound Sb_2Te_3 as excesses of either Sb or Te might diffuse into the CdTe. Finally, care must be taken to eliminate the formation of metastable crystalline modifications which are unknown in the bulk system as described by the phase diagram Sb–Te. In this work, the effect of substrate temperature on the material quality has been investigated.

In general, phase boundary effects play an important role for the transport across the solid–solid interface [20] for example by chemical reactive transport processes. Exchange processes can act to degrade the intermediate telluride layer, for example by consuming it (interdiffusion) or by the formation of isolated elemental or alloy phases embedded within the Sb_2Te_3 layer. The way that these compounds affect the contact properties is of considerable interest for a reliable contact technology for this kind of thin film solar cells. For that reason criteria concerning the chemical stability of a metal/Sb_2Te_3 interface have to be discussed in view of the choice for the best suited metal based on thermodynamic calculations. Phase diagrams of the ternary

system Sb–Te-metal and the kinetics of the presumed reactions occurring at the metal/Sb_2Te_3 interface have additionally to be taken into account.

To study the formation of alloys at the metal/Sb_2Te_3 interface dense sputtered Ni/Sb_2Te_3 and Mo/Sb_2Te_3 layers were used for kinetic test reactions for this kind of metal/telluride contact systems. The morphology of the reaction zone between thin polycrystalline layers depends on the nucleation rate and on the phase distribution of the reaction products at the interface. The combination of thermodynamic calculations and the results of the exchange reaction tests in this work were done to provide a better understanding of the chemical stability and provides a framework for the development of new metal/telluride back contact systems for CdTe/CdS thin film solar cells and modules.

2. Experimental

Soda-lime glass was used as substrates for the layers grown for the kinetic test reactions. Sb_2Te_3 and Sb–Te layers with a thickness of 2.0–2.2 μm were deposited by DC-sputtering ($P = 0.3\,W/cm^2$) using a deposition rate of 17 Å/s employing an Sb_2Te_3 target (99.99%, supplied by Cerac Inc.) in an atmosphere of 3×10^{-3} mbar of argon. The substrate temperature was varied in the range 293–523 K.

Sb–Te and Sb_2Te_3 layers deposited at 293 and 461 K were covered with Ni layers by DC-sputtering ($P = 6.5\,W/cm^2$) with an average thickness of 150 nm using a deposition rate of 510 Å/s in an atmosphere of 5×10^{-3} mbar of argon. The substrate temperature was held at 356 K while sputtering. The Ni target was supplied by Cerac Inc. (99.995%).

Mo layers with a thickness of 160–200 nm were deposited by DC-sputtering from a target supplied by Cerac Inc. (99.95%) with a deposition rate of 2.4 Å/s in an atmosphere of 8×10^{-3} mbar of argon. The substrate temperature was held at 298 K.

The kinetic test reaction samples were heat treated in a tubular furnace under an atmosphere of nitrogen to avoid oxide formation. The reaction temperature was varied between 373 and 573 K. After 7–12 d the samples were cooled under a nitrogen atmosphere. The X-ray diffraction (XRD) measurements (Philips PW 1800) of the layer samples were performed in a Bragg–Brentano $\theta-2\theta$ geometry employing $CuK_{\alpha 1}$ ($\lambda = 1.54056$ Å) radiation. The layers were characterised in a range of 10–100° 2θ using a step width of 0.02° with a detection time of 7 s/step. The XRD patterns were identified using JCPDS data cards. To get a higher accuracy of the positions of the reflections the layers were also characterised by the Guinier method. The layers were removed from the glass substrates and pulverised. The Guinier film was exposed for 8–10 h employing the $CuK_{\alpha 1}$ radiation generated by an acceleration voltage of 40 kV and an anode current of 30 mA. The positions of the reflections were evaluated by using a commercial Guinier viewer.

The Hall mobility of the polycrystalline Sb–Te material was determined by measuring the change of the resistance when a magnetic field of 0.8 T was applied perpendicular to the $2 \times 2\,cm^2$ square sample. The sample geometry was corrected by introducing a geometric factor of 0.7. The current was ≈ 1 mA. To examine the

homogeneity of the sample the polarity of magnetic field was reversed. The 4-point van der Pauw method was used to evaluate the sample resistivity using metal contacts (1 mm^2) on the middle of each edge.

3. Results and discussion

3.1. Sb–Te and Sb_2Te_3 characterisation

The Sb–Te phase diagram of bulk material is characterised by the presence of two eutectica and a congruent melting intermediate compound Sb_2Te_3 [21–26]. Sb_2Te_3 belongs to the family of layered-type semiconductors showing a small existence region [27,28]. Two phases, δ and γ Sb–Te have extended ranges of homogeneity and are described by two sub-lattices of $Sb_2(Te, Sb)_3$ [21]. One sub-lattice is occupied by Sb atoms only and the other one by a mixture of Sb and Te atoms. The Sb_2Te_3 is isomorphous with Bi_2Te_3 and belongs to the space group $R\bar{3}m$ (tetradymite type) containing 3 Sb_2Te_3 units per hexagonal cell [29]. The structure is described by the alternation of layers of Sb and Te perpendicular to the threefold axis [24,30].

The Sb–Te and Sb_2Te_3 layers deposited in this work were sputtered from an Sb_2Te_3 target. The target material contains slight amounts of excess Te and Sb which were identified by XRD measurements and reference to the JCPDS database.[1,2] The pattern of Sb_2Te_3, i.e. the major component of the target is identical with the Sb_2Te_3 JCPDS pattern [29].[3] Sputtering at room temperature leads to an Sb–Te phase which is not known from the Sb–Te bulk phase diagram. The crystal structures of β, δ and γ Sb–Te [26][4,5] are still unknown [21,22]. Stegherr [27,28] describes the existence region ε with several hexagonal crystal structures of Sb–Te phases which differ in the stacking of the layers. The XRD pattern of layers sputtered at room temperature (Fig. 1) belongs to an Sb–Te phase having the same stoichiometry as Sb_2Te_3 but the reflection positions are not identical with the values of Sb_2Te_3 [29] (see footnote 3), nor with any of the β and γ Sb-Te modifications (see footnote 4 and 5). This crystalline Sb–Te phase cannot be described by either an Sb-rich Te, or a Te-rich Sb alloy phase following Vegard's rule. This Sb–Te phase is described by *d* values and intensities as shown in Table 1 based on Guinier measurements. It cannot be excluded that between the crystalline Sb–Te additional Sb–Te alloys are present in an amorphous state and so are undetectable. However, precipitations of separate alloys are not found by SEM. From work on the Sb–Te system for use in re-writeable optical recording media [25] it is known that Sb–Te films deposited at room temperature comprise a mixture of an amorphous Sb–Te phase together with crystalline Sb_2Te_3 [31]. Upon annealing this Sb–Te phase transforms to monophase

[1] JCPDS 5-0562 (Sb).
[2] JCPDS 4-0554 (Te).
[3] JCPDS 15-874 (Sb_2Te_3).
[4] JCPDS 15-41 (β Sb–Te).
[5] JCPDS 15-42 (γ Sb–Te).

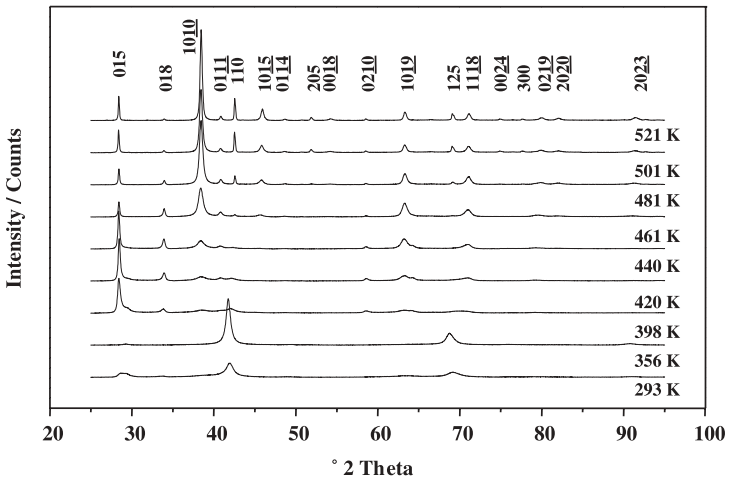

Fig. 1. XRD patterns of sputtered Sb–Te and Sb_2Te_3 layers: The substrate temperature was varied in a range of 293–521 K.

Table 1
Guinier measurement of Sb–Te layers sputtered at 293 K

Sb–Te d/Å	I/I_0
3.0518	Medium
2.1812	Weak
1.7958	Medium–strong
1.5784	Strong
1.1538	Strong
1.0136	Weak–medium
0.9788	Medium–strong
0.8839	Weak–medium
0.8264	Medium
0.7926	Weak–medium

Sb_2Te_3, the conversion following a simple Arrhenius relation with an activation energy of 2 eV [25,32]. For substrate temperatures below 398 K for sputtering the XRD line position of the Sb–Te described above remain at the same values. This indicates that the observed Sb–Te phase may be described as a defined alloy and no new phases appear.

At substrate temperatures above 398 K the XRD pattern of the material has the same reflection positions as Sb_2Te_3 identified by JCPDS [29] (see footnote 3). The pattern is characterised by one main and several broad peaks. The (0, 1, 5) peak is the most intense while the (1,0,$\underline{10}$) and the (1, 1, 0) remain broad with a low intensity. Raising the substrate temperature to 461 K sharpens the peaks indicating a better crystallinity of the material. The relative intensity of the peaks changes with (1,0,$\underline{10}$)

becoming the most intense. This is due to a change from a random orientation into a preferred orientation of the Sb_2Te_3 layer depending on the substrate temperature. At a substrate temperature of 501 K the complete Sb_2Te_3 pattern (footnote 3) can be observed. The pattern of the Sb–Te phase has disappeared leaving no separate alloy peaks between the Sb_2Te_3 peaks. The lattice parameters are determined by Guinier measurements at $a = 4.270$ Å and $c = 30.661$ Å for a hexagonal cell. The lattice parameters are slightly larger than reported from Sb_2Te_3 powder samples [23] (footnote 3). These results leads us to the conclusion that the Sb–Te alloy is a thermodynamically metastable precursor of Sb_2Te_3 with a transformation point between 356 and 398 K. The reason that this phase was not previously described in the literature can be that the Sb–Te alloy will be a specific thin film phase which will not appear in bulk material. For layers grown above 523 K it has been shown that the Sb_2Te_3 film looses more Te than Sb by re-evaporation according to the different vapour pressures of Sb and Te [12,33,34].

Fig. 2 illustrates the variation of the Hall mobility and the Hall carrier density as a function of the substrate temperature while sputtering the Sb–Te alloy. The Hall mobility increases with rising substrate temperature while the Hall carrier density reaches a broad maximum at temperatures above 443 K. This behaviour can be understood if we consider the formation of a stable crystalline Sb_2Te_3 alloy via a metastable Sb–Te phase. Conversion of amorphous precipitates into a crystalline phase may be responsible for a significant increase of the Hall mobility and Hall carrier density from room temperature to 398 K, where Sb_2Te_3 is observed first in a crystalline state. An increase in the Hall mobility even when the stable Sb_2Te_3 has been formed might be caused by reduction of the defect density, lowering of the material stress and perhaps the passivation of extended defects with an increase of the substrate temperature.

The Sb_2Te_3 layer used as a back contact adaptation layer has to fulfil two criteria: (i) a *dense* film of a *chemically stable* polycrystalline Sb_2Te_3 may act as a diffusion

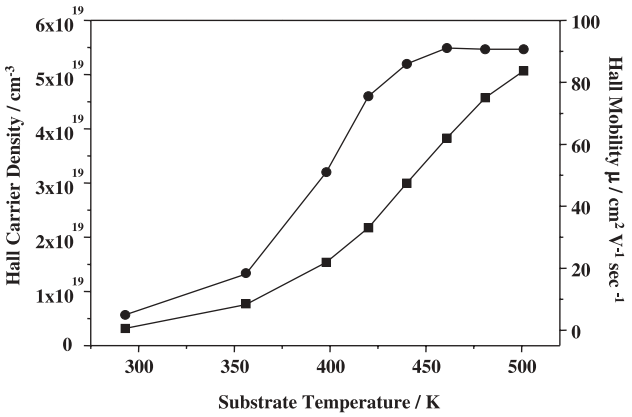

Fig. 2. Hall mobility and Hall carrier density of sputtered Sb–Te and Sb_2Te_3 layers: The substrate temperature was varied in a range of 293–521 K.

barrier for the back contact metal (Ni or Mo) and (ii) the p-doping of the Sb_2Te_3 caused by excess Te has to be high enough to allow tunnelling of the carriers. The necessary characteristics for a thin Sb_2Te_3 tunnel contact layer [35] will be satisfied if the Sb_2Te_3 layers are sputtered at substrate temperatures above 443 K. Usefulness of the Sb_2Te_3 layer as a diffusion barrier depends on a dense crystallinity of the polycrystalline material and has to be discussed in context with the chemical stability according to the back contact metal Ni or Mo, as described in the following sections.

3.2. Thermodynamic assessment of the chemical stability of Ni/Sb_2Te_3 and Mo/Sb_2Te_3 layers

3.2.1. General thermodynamic considerations

Chemically reactive transport processes across the metal/Sb_2Te_3 interface may form isolated elemental or alloy phases embedded within the Sb_2Te_3. For a better understanding of the chemical stability of the Ni/Sb_2Te_3 and Mo/Sb_2Te_3 interfaces thermodynamic data concerning the ternary phase diagrams of Sb–Te–Mo and Sb–Te–Ni [36], phase boundary equilibria and kinetic data due to real interactions in solid-state reaction pairs have to be considered. The morphology of the reaction zone depends on the nucleation rate and on the phase distribution of the products. Low nucleation rates lead to a high number of isolated precipitates of the product phase. The growth of pores caused by an increasing vacancy flux and agglomeration may destroy the back contact system by lowering the contact area. A dense arrangement of pores arising from the Kirkendall effect has been shown to be characteristic for the formation of reaction zones at chalcogenide phase boundaries [20]. The degradation of the back contact double-layer system is expected to be very sensitive by small stoichiometric deviations of the metal/Sb_2Te_3 interface caused by interdiffusion of the components Sb, Te, Mo and Ni, respectively. The formation of intermediate reaction products even on the surface of the Sb_2Te_3 may result in significant changes of the electrical characteristics of this kind of back contact depending on the ageing process of the solar cell.

We describe the alloy formation at the metal/Sb_2Te_3 interface while operating and ageing a CdTe/CdS solar cell by simple chemical reaction equations. Reactions including non-stoichiometric alloys are not considered but these alloys may lead to a more favoured pathway of chemical reactions. The main reactions leading to defined alloys are discussed with reference to thermodynamic data.

In general, the Gibb's free energy change ΔG of a chemical reaction is calculated by means of the equations:

$$\Delta G = \Delta H - T\,\Delta S, \tag{1}$$

$$\Delta G = -RT \ln k \tag{2}$$

using any available thermodynamic data of the enthalpy changes ΔH, the entropy changes ΔS and the equilibrium constant k. The ΔG data will give information about the feasibility of a presumed reaction for any temperature T: for reactions with $\Delta G < 0$ a spontaneous reaction is postulated, reactions with $\Delta G > 0$ are not taken

into account under these conditions. The temperature dependence of $\Delta_T H$ and S_T is considered by the equations:

$$\Delta_T H = \overset{\circ}{\Delta_T} H + \int_{T_0}^{T} C_P \, dT, \tag{3}$$

$$S_T = \overset{\circ}{S_T} + \int_{T0}^{T} C_P \frac{dT}{T} \tag{4}$$

while $\overset{\circ}{\Delta_T} H$ and $\overset{\circ}{S_T}$ represent the standard values of a component at a reference temperature of $T_0 = 298.15\,\mathrm{K}$ and at a standard pressure of $p_0 = 1\,\mathrm{bar}$. The heat capacity C_p is determined by a polynomial expression:

$$C_p = a + b \times 10^{-3}\, T + c \times 10^{6}\, T^{-2} + d \times 10^{-6} T^2 \tag{5}$$

in which a, b, c and d are tabulated polynomial coefficients [37,38].

Nevertheless, the presumed solid-state reaction in a chosen system may not occur for kinetic reasons even when the reaction will be possible energetically. In addition, we have to consider the very special situation of an interface solid-state reaction between sputtered polycrystalline layers which will be quite different to investigations using single crystal reaction pairs or milled powders. The kinetics of powder reactions and sputtered polycrystalline thin layers are mainly determined by the shape of individual grains, by the grain size distribution and by the packing density, respectively [39].

The Gibb's free energy of formation $\Delta_f{}^\circ G$ of Sb_2Te_3 from the elements is at standard conditions numerically very low ($-58.35\,\mathrm{kJ/mol}$) [38] and rises slightly with the temperature (Fig. 3). Using a stoichiometric Sb_2Te_3 layer without any excess of Sb or Te as an isolated phase, Ni- or Mo-tellurides and -antimonides are formed while consuming the Sb_2Te_3. These product alloys exist in a thermodynamic equilibrium described by ternary phase diagrams Sb–Te–Ni [36] and Sb–Te–Mo, respectively. Many of these alloys are located within the binary phase diagrams of Ni–Te [40–43], Ni–Sb [44–47], Mo–Te [48–50] and Mo–Sb [51,52], respectively. Reactions including non-stoichiometric phases are not considered because thermodynamic data are not available in detail for Ni/Sb_2Te_3 and Mo/Sb_2Te_3 systems. It is possible that these phases may lead to a more favourable pathway of a reaction of the back contact metal with Sb_2Te_3 [4]. Thermodynamic and crystallographic data of alloys within Ni–Sb–Te and Mo–Sb–Te systems used in this paper are summarised in Table 2. For some alloys belonging to the discussed systems there are no thermodynamic data available. The possibility that these alloys will appear in our investigations cannot be excluded.

For the Sb–Te phase described earlier in this paper there are no thermodynamic data available. The Sb–Te phase is metastable and it changes into Sb_2Te_3 by heat treatment. If this phase is not stable concerning chemical reactions with Ni or Mo, the products will be alloys similar to those formed by the reaction with Sb_2Te_3. In addition, no oxide formation is taken into account so in this paper the conditions of the ageing of encapsulated CdTe/CdS solar cells and modules are presumed.

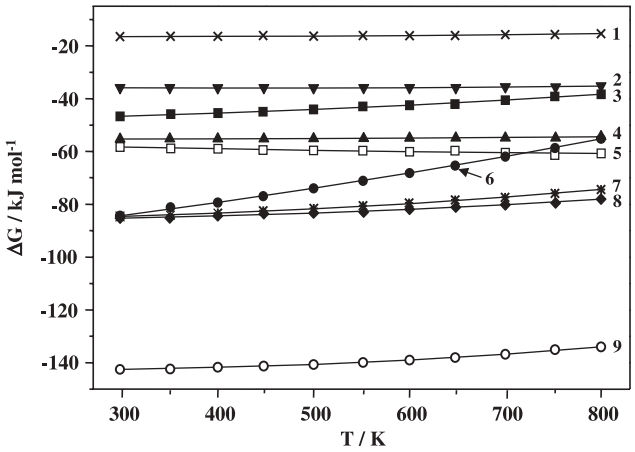

Fig. 3. Presumed chemical reactions in the Ni/Sb_2Te_3 system: ΔG as a function of T: (1) $Ni + 1/3\ Sb_2Te_3 \rightarrow NiTe + 2/3\ Sb$; (2) $Ni + Te \rightarrow NiTe$; (3) $Ni + 2/3\ Sb_2Te_3 \rightarrow NiTe_2 + 4/3\ Sb$; (4) $Ni + 1/2\ Sb_2Te_3 \rightarrow NiSb + 3/2\ Te$; (5) $2\ Sb + 3\ Te \rightarrow Sb_2Te_3$; (6) $Ni + Sb \rightarrow NiSb$; (7) $2\ Ni + Sb_2Te_3 \rightarrow Ni_2Te_3 + 2\ Sb$; (8) $Ni + 2\ Te \rightarrow NiTe_2$; and (9) $2\ Ni + 3\ Te \rightarrow Ni_2Te_3$.

3.3. *Ni/Sb–Te and Ni/Sb_2Te_3: thermodynamic assessment and kinetic tests*

The thermodynamic calculations (Table 2, Fig. 3) show that the main chemical reactions at the Ni/Sb_2Te_3 interface will lead to the formation of NiTe, $NiTe_2$, Ni_2Te_3 and Ni_9Te_{10} as defined alloys while separating the Sb following the formal stoichiometric equation. These reactions show negative values of ΔG so we have to presume that these reactions are possible by energetic reasons. For Ni-antimonides there are only thermodynamic data available concerning the formation of NiSb which shows a negative value of ΔG. In general, for this system the absolute values of ΔG depend on the chosen temperature (Fig. 3). Each of these postulated chemical reactions may occur spontaneously at the Ni/Sb_2Te_3 interface even while sputtering the Ni onto the Sb_2Te_3 surface. Solar modules in the field operate at a temperature of up to a range of 353–373 K. From the thermodynamic data it is therefore expected that Ni diffuses into the Sb_2Te_3 layer. Grain boundary diffusion will be the most favoured mechanism of diffusion but bulk diffusion may become more significant as a result of operating the solar module for many years. Close to the Ni/Sb_2Te_3 interface Ni will enrich the grain boundaries of the polycrystalline Sb_2Te_3 material while forming stable alloys. The diffusion of Sb or Te into the Ni layer will be much slower because Sb or Te has to be liberated from a stable Sb_2Te_3 lattice. Therefore, the main reaction zone of the three compounds is located within the Sb_2Te_3 layer. While migrating into the bulk of the Sb_2Te_3, Ni will diffuse using the Te or Sb sub-lattice or along extended defects of the Sb_2Te_3 grains. The stoichiometric condition of interdiffusion processes in the bulk material cannot be satisfied exactly as the diffusivities of the migrating species Ni, Sb and Te are all different even if the components use the same sub-lattice for migration. This will

Table 2
Thermodynamic and crystallographic data for stoichiometric alloys located in Sb–Te, Ni–Te, Ni–Sb, Ni–Te–Sb, Mo–Te, Mo–Sb and Mo–Te–Sb phase diagrams

Compound/alloy	$\Delta_f^\circ H$ (kJ/mol)	S°(J/K mol)	$\Delta_f^\circ G$ (kJ/mol)	C_p (J/K mol)	k_p	Space group	Prototype	JCPDS data base	References
Sb	0	45.52	0	25.23	—	R $\bar{3}$ m	W	5-562	[37,53]
Te	0	49.71	0	25.70	—	$P3_121$	γ-Se	4-554	[37,53]
Sb_2Te_3	−56.48	246.43	−58.35	128.72	1.7×10^{10}	R $\bar{3}$ m	Bi_2Te_3	15-874	[24,29,30,38,54,55]
β Sb-Te								15-41	[22,55]
γ Sb-Te								15-42	[26,55]
Ni	0	29.87	0	26.24	—	Fm $\bar{3}$ m	Cu	4-850	[37,53,56]
								45-1027	
NiTe	−35.65	80.12	−35.87	52.85	1.9×10^6	$P6_3/mmc$	NiAs	17-502	[41,43,54,55,57]
								38-1393	
$NiTe_{1.1}$	−58.16	84.06	−58.08	54.79	1.5×10^{10}				[38]
$NiTe_2$	−87.86	120.41	−85.34	76.27	8.9×10^{14}	P $\bar{3}$ m1	CdI_2	8-4	[41,55,57]
Ni_2Te_3	−144.77	200.91	−142.58	128.10	9.5×10^{24}				[57]
Ni_3Te_2						$P2_1/m$		19-848	[55]
Ni_3Te_2						P $\bar{4}$ m2		19-846	[55]
								23-1279	
Ni_9Te_{10}	−515.89	757.21	−513.91	496.02	1.1×10^{90}				[57]
NiSb	−83.68	78.24	−84.53	49.70	6.5×10^{14}	$P6_3/mmc$	NiAs	2-783	[38,44,54,55,58]
								41-1439	
$NiSb_2$						Pnnm	FeS_2	25-1083	[46,54,55,58]
								4-687	
$NiSb_7$						Pm $\bar{3}$ m	Po		[55]
Ni_3Sb						Pmmm	β-Cu_3Ti	25-50	[47,54,55,58]
Ni_5Sb_2						C	Ni_5Sb_2	25-49	[47,54,55,58]
								32-41	
								32-947	
Ni_7Sb_3									[54,58]
$Ni_{15}Sb$									[54,58]
Ni_9Sb						Fm $\bar{3}$ m	Cu		[55]
$Ni_{23}Sb_2$						Fm $\bar{3}$ m	Cu		[55]
Ni_2SbTe						$P6_3/mmc$	NiAs		[36,55]
Mo	0	28.61	0	23.51	—	Im $\bar{3}$ m	W	4-809	[37,53,56]
								42-1120	
α-$MoTe_2$	−80.14	115.38	−76.37	76.83	2.4×10^{13}	$P6_3/mmc$	MoS_2	15-658	[48,50,54,55,57,59]
β-$MoTe_2$	−80.14	115.38	−76.37	76.83	2.4×10^{13}	$P2_1/m$	$MoTe_2$		[48,54,55,57,59]
Mo_3Te_4	−162.95	267.51	−157.84	179.54	4.6×10^{27}	R $\bar{3}$	Mo_3Se_4	23-1257	[48,54,55,59]
$Mo_{49}Te$						Im $\bar{3}$ m	W		[55]
Mo_3Sb_7						Im $\bar{3}$ m	Ge_7Ir_3	19-807	[54,55]

cause an uncompensated flux of vacancies in the Sb_2Te_3 lattice which will lead to a higher instability and to a higher tendency of the formation of separate agglomerations. These agglomerations might contain Ni, Sb, Te, their alloys and solid solutions, respectively. All precipitates are defined by their existence region of the ternary Sb–Te–Ni phase diagram [36]. If a reaction between Sb_2Te_3 and the back contact metal is possible (determined by thermodynamic and kinetic reasoning) the interdiffusion of the three participating compounds Sb, Te and Ni determines the rate of the reaction product formation.

As a rule of thumb we expect that the reaction with the numerically highest negative value of ΔG to be the most favoured reaction of the Ni/Sb_2Te_3 system. In this case, we presume the formation of a separate Ni_2Te_3 alloy to be preferred over the formation of precipitates of NiSb, $NiTe_2$ and NiTe, respectively, if we look at the Sb_2Te_3 consuming reactions only. As a result of the Ni-telluride and Ni-antimonide formation we liberate Sb or Te following the formal chemical reaction equation. Segregations of Sb or Te will react with any of the migrating components. These reactions are described by the formation of Sb_2Te_3, Ni_xTe_y and Ni_xSb_y, respectively, from the elements. As shown in Fig. 3 the formation of Sb_2Te_3 is more favoured than the formation of NiTe from the elements only, so we expect Ni alloys most if we presume the same possibility of occurrence of the three compounds in one place. By energetic reasons Ni_2Te_3 is the most favoured alloy forming from the elements. The conclusion of the theoretical thermodynamic assessment is that in general, we expect chemical changes of the Sb_2Te_3 layer while forming precipitates of Ni_2Te_3 as a preferred reaction product. Side reactions may lead to any of the described alloys depending on local conditions of the solid-state system. If we have to discuss an Sb_2Te_3 layer containing a slight amount of Sb or Te within the Sb_2Te_3 we will have the same situation as described before. Sb_2Te_3, Sb and Te will react with Ni forming stable alloys following the same thermodynamic criteria.

The reaction products of the kinetic test reactions for sputtered Ni/Sb_2Te_3 layers are identified by XRD measurements using the crystallographic data summarised in Table 2. To imitate the degradation of the Ni/Sb_2Te_3 back contact system while operating an encapsulated solar module the sputtered double layers were annealed in a nitrogen atmosphere. If the temperature of an operating solar module is presumed at about 353–373 K the kinetic test reaction of the Ni/Sb_2Te_3 layer annealed at 373 K is a comparable system. As shown in Fig. 4 we identified from a sample which has been annealed at 373 K for 7 d the XRD patterns of Sb_2Te_3 (see footnote 3) and Ni[6] exclusively. This pattern is identical to the untreated sample because no significant increase or decrease of the reflections nor a peak shift is observed. This means that Ni is not introduced into the Sb_2Te_3 lattice in quantities high enough to change the lattice parameters.

The pattern of hexagonal $NiTe_2$[7] ($P\bar{3}m1$) appears very clearly if the sample is annealed at 473 K. The (0, 0, 2) peak is most intense. The pattern of the Sb_2Te_3 is still identified while the (1,0,$\underline{10}$) peak is still the strongest. The (0, 1, 5) and the (0, 1, 8)

[6] JCPDS 45-1027 (Ni).
[7] JCPDS 8-4 ($NiTe_2$).

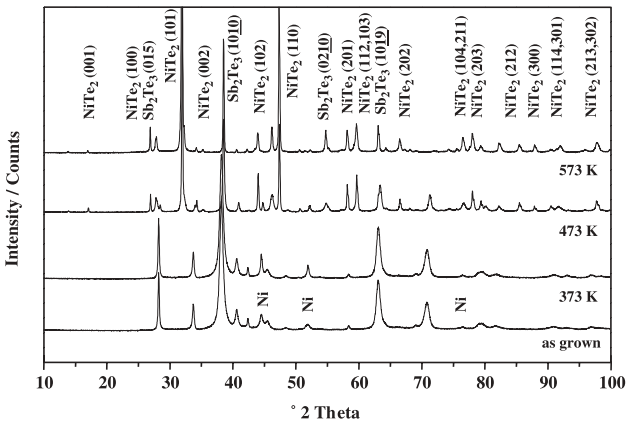

Fig. 4. Ni/Sb_2Te_3 double-layer system: XRD patterns of kinetic test reactions as grown and annealed in a temperature range of 373–573 K for 7 d.

peak decrease in intensity while broadening but remain at the same reflection positions. This is correlated with the ongoing in-diffusion of Ni and consumption of the Sb_2Te_3 layer at higher temperatures. Between the Sb_2Te_3 and $NiTe_2$ peaks the pattern of Ni still remains. It is remarkable that no other alloy can be identified not even a Ni-telluride[8,9,10] or a Ni-antimonide.[11,12,13,14,15,16] This is consistent to the thermodynamic assessment and demonstrates that the kinetic of the reaction allows the formation of $NiTe_2$ as the favoured reaction product. We cannot rule out the possibility of the formation of amorphous precipitates of Sb, Te or the other presumed alloys embedded in the Sb_2Te_3 matrix. These products are not detectable by XRD measurements. The reflection positions of the Sb_2Te_3 peaks do not shift as their intensity decrease, and the lattice of the Sb_2Te_3 is not changed by Ni. A change in doping of the remaining Sb_2Te_3 layer cannot be excluded. This might be important for the use of Sb_2Te_3 layers as a tunnel contact. At an annealing temperature of 573 K we observe the $NiTe_2$ pattern between the Ni and the Sb_2Te_3 pattern which is still identified by the (1,0,$\underline{1}$0) as the most intense peak. The whole system did not reach the thermodynamic equilibrium at this temperature.

Schmidt et al. [17] reported the formation of NiTe using Sb_2Te_3 and Ni powder samples annealed in the range 523–573 K. They did not find any $NiTe_2$, which was

[8] JCPDS 38-1393 (NiTe).
[9] JCPDS 19-846 (Ni_3Te_2).
[10] JCPDS 19-848 (Ni_3Te_2).
[11] JCPDS 41-1439 (NiSb).
[12] JCPDS 25-1083 ($NiSb_2$).
[13] JCPDS 25-50 (Ni_3Sb).
[14] JCPDS 32-41 (Ni_5Sb_2).
[15] JCPDS 32-947 (Ni_5Sb_2).
[16] JCPDS 25-49 (Ni_5Sb_2).

shown by differential thermal analysis (DTA) and XRD measurements. This result indicates the different appearance of the reaction pairs. Milled and mixed powders allow the coverage of the Sb_2Te_3 grains with Ni particles while the system of sputtered thin films described in this work assumes the Ni diffusion into a dense Sb_2Te_3 layer to initiate the formation of a detectable reaction zone or product.

We expect a similar product formation depending on the ternary phase diagram Sb–Te–Ni while using sputtered Sb–Te phases as a substrate for Ni test reactions. The thermodynamic data for the Sb–Te phase described in this paper are not available but we presume that this phase is less stable than the Sb_2Te_3 compound. Less stable Sb–Te phases will react more easily with the back contact metal even when these reactions are energetically less favoured. The Sb or Te in a metastable Sb–Te alloy has a lower lattice energy and can be freed easily. The product formation has to be described in a similar way as using Sb_2Te_3. The XRD pattern of kinetic test reactions using Sb–Te sputtered at room temperature and covered with a Ni layer are demonstrated in Fig. 5. After annealing the sample at 373 K for 7 d no significant changes in the XRD pattern are observed. The Sb–Te phase is still a stable modification at this temperature. Heat treatment at 473 K leads to a characteristic $NiTe_2$ pattern and an Sb_2Te_3 pattern caused by the transformation of the Sb–Te phase. While forming stable alloys by chemical reactions between the Sb–Te phase and Ni, the transformation of Sb–Te into the stable Sb_2Te_3 modification is identified as a parallel concurrence reaction. This transformation is not influenced by the appearance of Ni. This leads us to the conclusion that Ni is not incorporated into the bulk Sb_2Te_3 in a higher concentration than a doping level. A large Ni incorporation may have caused a significant lattice widening or diminishing effect by shifting the reflection positions. We obtain the same alloy products as using Ni/Sb_2Te_3 for kinetic tests. At 473 K the Sb–Te changes completely into the stable

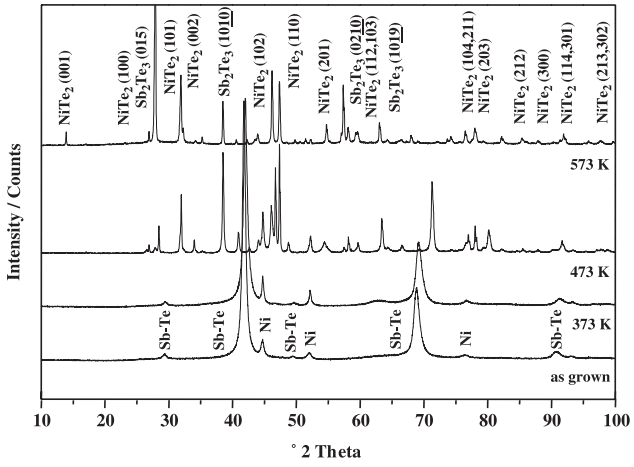

Fig. 5. Ni/Sb–Te double-layer system: XRD patterns of kinetic test reactions as grown and annealed in a temperature range of 373–573 K for 7 d.

Sb_2Te_3 modification while reaching the thermodynamic equilibrium. We presume that this transformation has been finished when Ni is still diffusing into the Sb–Te layer. Then Ni will meet even more Sb_2Te_3 than Sb–Te as a reaction partner in the bulk of the layer. Now we determine $NiTe_2$ as a reaction product following the argumentation as mentioned above while using the stable Sb_2Te_3 as a substrate. Only in the beginning of the heat treatment Ni will react with the Sb–Te phase, and this is located mainly at the Ni/Sb–Te interface. It cannot be excluded that different intermediate reaction products—crystalline or amorphous—will appear. They will change into more stable alloy phases determined by the thermodynamic equilibrium. These pathways of alloy formation cannot be proofed by XRD measurements.

3.4. *Mo/Sb–Te and Mo/Sb_2Te_3: thermodynamic assessment and kinetic tests*

From the thermodynamic point of view we identify α-$MoTe_2$, β-$MoTe_2$ and Mo_3Te_4 as defined alloys in the Mo–Te system [48–50]. In addition, a $Mo_{49}Te$ phase is described [55]. For the Mo–Sb phase diagram [51,52] containing Mo_3Sb_7 as a stable alloy no thermodynamic data are available. We use ΔG as a measure of the possibility of presumed chemical reactions at the Mo/Sb_2Te_3 interface following the principles of the thermodynamic assessment as described above. The formation of Mo_3Te_4 and α, β-$MoTe_2$ while consuming the Sb_2Te_3 release negative values of ΔG (Fig. 6) and will occur spontaneously subject to kinetic limitations. The reaction leading to Mo_3Te_4 has the highest negative value of ΔG and so Mo_3Te_4 is expected as a main reaction product. This value of ΔG is in the same magnitude than for the most favoured reactions within the Ni/Sb_2Te_3 system. This leads us to the conclusion that from the thermodynamic point of view the Mo/Sb_2Te_3 system has a comparable chemical stability as the Ni/Sb_2Te_3 system. After annealing an Sb_2Te_3 layer covered with Mo the XRD reflection patterns of Sb_2Te_3 and Mo[17] are still observed. Heat treatment at 573 K leads to no significant changes in the XRD pattern. The annealing causes only a sharpening of the peaks of Sb_2Te_3 due to better crystallinity. The pattern of the Sb_2Te_3 is exactly identical with the pattern illustrated in Fig. 1. No lattice widening or diminishing from the presence of Mo within the Sb_2Te_3 lattice is detectable. While using the thermodynamically less stable Sb–Te as starting material for the kinetic test reaction no additional reflection peaks of the Mo_3Te_4,[18] the α, β-$MoTe_2$[19] and the Mo_3Sb_7[20] pattern are found. Only the typical transformation of the Sb–Te phase into the stable Sb_2Te_3 phase depending on the temperature is observed. This result is explained by the fact that the diffusion velocity of the Mo into an Sb–Te or Sb_2Te_3 layer is so low that an alloy formation is not detectable after 12 d. If Mo is migrating into the Sb_2Te_3 layer using extended defects and grain boundaries it might have a negligible tendency for bulk diffusion. Alloys formed at the surface of the Sb_2Te_3 grains might be amorphous and for that reason not

[17] JCPDS 4-0811 (Mo)
[18] JCPDS 23-1257 (Mo_3Te_4).
[19] JCPDS 15-658 ($MoTe_2$).
[20] JCPDS 19-807 (Mo_3Sb_7).

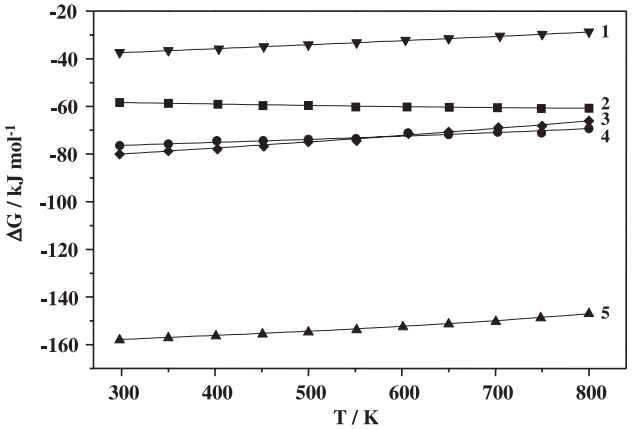

Fig. 6. Presumed chemical reactions in the Mo/Sb_2Te_3 system: ΔG as a function of T: (1) $Mo + 2/3\ Sb_2Te_3 \rightarrow MoTe_2 + 4/3\ Sb$; (2) $2\ Sb + 3\ Te \rightarrow Sb_2Te_3$; (3) $3\ Mo + 4/3\ Sb_2Te_3 \rightarrow Mo_3Te_4 + 8/3\ Sb$; (4) $Mo + 2\ Te \rightarrow MoTe_2$; and (5) $3\ Mo + 4\ Te \rightarrow Mo_3Te_4$.

detectable by XRD measurements. We assume that an alloy formation detectable by XRD measurements depends on the penetration of the Mo into the bulk of the Sb_2Te_3 grains which allows the precipitation of an alloy phase in a crystalline state. However, as the values of ΔG for Sb_2Te_3 consuming reactions are so large, it cannot be ruled out that a small amount of any reaction product will appear in an amorphous state concentrated at the Mo/Sb_2Te_3 interface. The best explanation for the results of these kinetic test reactions is that formation of the Mo-tellurides and Mo-antimonides require high activation energies and these are not overcome in the chosen reaction conditions.

3.5. Ni/Sb_2Te_3 and Mo/Sb_2Te_3 layers as back contact systems for CdTe/CdS thin film solar cells

High-efficiency CdTe/CdS solar cells show decreases in the photovoltaic parameters like efficiency η, open-circuit voltage V_{OC}, short-circuit current J_{SC} and fill factor FF. Junction degradation, degradation of the electrical contacts to the CdTe absorber layer and shunting are proposed to be responsible as the main degradation pathways [60]. Often the $J-V$ characteristic of the cell is influenced by the development of a characteristic "roll-over" at high forward bias [61].

One aspect of the degradation mechanism of metal/Sb_2Te_3 back contacts is now easily understood by the model of the consumption of the intermediate Sb_2Te_3 layer during alloy formation as mentioned above. Even changing the stoichiometry of the back contact metal/Sb_2Te_3 interface and the lowering of the contact area will support the back contact degradation. Junction degradation may in principle be caused by the contamination with impurities from the front and back contact accumulating in the CdS window layer near the space charge region. It is suggested

that grain boundary diffusion is a very likely mechanism for the impurity transport into the device. A temperature in a range of 353–373 K while operating a CdTe/CdS solar cell or module will enhance the diffusion of metals into the CdTe absorber layer depending on the characteristic diffusion velocity and diffusion mechanism of the metal.

Impurities can be active as dopants, create highly conductive grain boundary channels and cause shunting paths through the junction. The distribution of the internal field can be changed by connecting the front and the back of the CdTe grains [61]. In this case, a dense Sb_2Te_3 layer will act as a diffusion barrier for Ni and Mo. If alloy formation caused by a chemical reaction of the Sb_2Te_3 with Ni or Mo occur, the migration velocity of the metal diffusion into the CdTe absorber is reduced. These solar cells will show a better long-term stability depending now on the changes in the properties of the Sb_2Te_3 tunnel contact caused by changes in doping. Only for Ni we observe alloy formation following the chemical reactions of Ni with Sb–Te or Sb_2Te_3. Ni will reach the absorber layer when the Sb_2Te_3 is consumed by the last alloy formation and Ni is known as a slow diffuser in bulk CdTe. From this point the alloy forming diffusion barrier does not exist any more. There after the solar cell will show a significant worsening of its characteristic cell parameters as efficiency η and fill factor FF. Using Mo no alloy formation with Sb_2Te_3 and Sb–Te is observed. If Mo is a slow diffuser in the Sb_2Te_3 layer, then CdTe/CdS cells employing a Mo/Sb_2Te_3 back contact will show a better long-term stability. However, should a slight amount of Mo pass the Sb_2Te_3 layer and so enter the CdTe absorber, then degradation of the solar cell performance can be expected. This assumption is confirmed by Romeo et al. [13–16] and Beier et al. [62]. The migration of Mo into the CdTe is associated with the formation of high trap densities in the CdTe bulk material, thus adversely affecting the internal electric field distribution [63].

The alloy formation as a result of chemical reactions of Sb_2Te_3 with Ni will separate Sb or Te following the formal reaction equation. Sb or Te will be precipitated as a separate phase or might react with Ni. Liberated Sb or Te will have a much higher diffusion tendency into the CdTe absorber layer than Sb or Te fixed in a stable Sb_2Te_3 lattice. Sb substitutes Te (Sb_{Te}) in CdTe and causes p-doping [64–66]. Diffusion of Te liberated from the Sb_2Te_3 tunnel contact layer enriches the CdTe grain boundaries with excess Te and changes the doping level of the p-CdTe absorber. This will change the band bending at the Sb_2Te_3/CdTe interface [60]. As we know from the diffusion characteristics of Cu and Au in CdTe single crystals, an excess of Te enhances the diffusion velocity of impurities which can be explained by the diffusion mechanism along extended defects of Te precipitates or by complex formation with V_{Cd} [67]. The simultaneous diffusion of Sb and Te into the CdTe absorber will both increase the p-doping [64]. Within CdS the Sb is expected to decrease the n-doping and it will make the CdS more resistive. Combined with the assumed temperature of 353–373 K while operating a solar module outdoors the degradation by electromigration and ionic diffusion caused by the internal electric field will increase the degradation rate. Within the CdS layer impurities like Sb, Ni and Mo will accumulate which has been shown by SIMS measurements [60,62]. Changes in crystal structure, photosensitivity and a decrease in the band gap of the

CdS cannot be excluded. As a result of this accumulation, the CdS window will be more influenced than the CdTe absorber by impurities. Then the short-circuit current J_{SC} will be affected by degradation due to the impurity constellation. Overall the back contact is considered as a most important source of impurities that may act in the CdTe, CdS and p/n junction so as to degrade the solar cell performance. Control of the back contact material stability is therefore critical in ensuring long-term device stability.

4. Conclusion

Sputtering at room temperature from an Sb_2Te_3 target containing a slight amount of free Sb and Te leads to a metastable Sb–Te thin film modification. This Sb–Te alloy will transform into the stable Sb_2Te_3 phase with a transformation point between 356 and 398 K. Using a stable Sb_2Te_3 phase as a tunnel contact for CdTe/CdS solar cells the substrate temperature while sputtering has to be above 420 K.

Exchange processes at the Sb_2Te_3/metal interface destroy the intermediate telluride layer via consumption of the Sb_2Te_3 and by the formation of isolated elemental or alloy phases embedded in the Sb_2Te_3 matrix. Thermodynamic assessments of Sb–Te–Ni and Sb–Te–Mo systems lead to the conclusion that Ni/Sb_2Te_3 and Mo/Sb_2Te_3 thin film layers are not chemically stable while forming defined alloys at the interface. Sputtered double layer samples are used for kinetic test reactions as an indicator for chemical stability. Using Ni/Sb_2Te_3 layers the formation of $NiTe_2$ is proofed as a crystalline reaction product by XRD measurements. The Mo/Sb_2Te_3 system is chemically stable during heat treatment presumably as a consequence of high activation energies for the chemical conversion or the low diffusion velocity of Mo in a polycrystalline Sb_2Te_3 matrix. The transformation of Sb–Te into Sb_2Te_3 is observed as a side reaction of the heat treatment. Sb_2Te_3 sputtered at temperatures above 420 K in combination with Mo overlayers are expected to be a suitable back contact system for CdTe/CdS thin film solar cells and modules and should offer improved long-term stability.

Acknowledgements

The Bundesministerium für Bildung, Wissenschaft und Technologie BMWi (Contract No. 0329787) and the EU (Contract No. J0R39802) is acknowledged for financial support. Technical assistance was provided by O.J. Bartelt, Institute for Mineralogy, University of Hannover, Germany, (Guinier, XRD measurements), by M. Köntges, ISFH Hannover, Germany, (sample sputtering, Hall measurements) and by the Faculty of Physics, Carl-von-Ossietzky University of Oldenburg, Germany, (Hall measurements). Dr. K. Durose, Department of Physics, University of Durham, UK, is gratefully acknowledged for stimulating discussions and critical reading of the manuscript.

References

[1] A.L. Fahrenbruch, Sol. Cells 21 (1987) 399.
[2] Y. Marfaing, Thin Solid Films 387 (2001) 123.
[3] B. Depuydt, M. Burgelman, M. Castelyn, A. Niemegeers, A. Verveat, Proceedings of the 13th European Conference on Photovoltaic Solar Energy Conversion, Nice, 1995, p. 593.
[4] B.E. McCandless, J.E. Philipps, J. Titus, Second World Conference on Photovoltaic Solar Energy Conversion, Vienna, 1998, p. 448.
[5] J.P. Ponpon, Solid State Electronics 28 (7) (1985) 689.
[6] A. Rohatghi, R. Sundharsanan, S.A. Ringel, M.H. MacDougal, Sol. Cells 30 (1991) 109.
[7] F.A. Ponce, R. Sinclair, R.H. Bube, Appl. Phys. Lett. 39 (12) (1981) 951.
[8] V.P. Singh, O.M. Erickson, J.H. Chao, J. Appl. Phys. 78 (7) (1995) 4538.
[9] T.L. Chu, S.S. Chu, S.T. Ang, J. Appl. Phys. 58 (8) (1985) 3206.
[10] D.W. Niles, X. Li, P. Sheldon, J. Appl. Phys. 77 (9) (1995) 4489.
[11] D.L. Bätzner, A. Romeo, H. Zogg, R. Wendt, A.N. Tiwari, Thin Solid Films 387 (2001) 151.
[12] N. Romeo, A. Bosio, R. Tedeschi, V. Canevari, Mater. Chem. Phys. 66 (2000) 201.
[13] N. Romeo, A. Bosio, R. Tedeschi, V. Canevari, Thin Solid Films 361–362 (2000) 327.
[14] N. Romeo, A. Bosio, R. Tedeschi, A. Romeo, V. Canevari, Second World Conference on Photovoltaic Solar Energy Conversion, Barcelona, 1997, p. 2351.
[15] N. Romeo, A. Bosio, R. Tedeschi, V. Canevari, Second World Conference on Photovoltaic Solar Energy Conversion, Vienna, 1998, p. 446.
[16] N. Romeo, A. Bosio, R. Tedeschi, A. Romeo, V. Canevari, Sol. Energy Mater. Sol. Cells 58 (1999) 209.
[17] T. Schmidt, K. Durose, C. Rothenhäusler, M. Lerch, Thin Solid Films 361-362 (2000) 383.
[18] D.S. Boyle, K. Durose, R. Wendt, D. Bonnet, Proceedings of the 16th European Conference on Photovoltaic Solar Energy Conversion, Glasgow, 2000.
[19] A. Abken, O. Bartelt, M. Köntges, K. Oehlstrom, R. Reineke-Koch, S. Ulrich, Proceedings on the 16th European Conference on Photovoltaic Solar Energy Conversion, Glasgow, 2000.
[20] V. Leute, Solid State Ionics 17 (1985) 185.
[21] G. Gosh, H.L. Lukas, L. Delaey, Z. Metallkunde 80 (10) (1989) 731.
[22] N.Kh. Abrikosov, L.V. Poretskaya, I.P. Ivanova, Russ. J. Inorg. Chem. 4 (1959) 1163.
[23] E. Dönges, Z. Anorg. Allg. Chem. 265 (1951) 51.
[24] T.L. Anderson, H.B. Krause, Acta Cryst. B 30 (1974) 1307.
[25] S. Fujimori, S. Yagi, H. Yamazaki, N. Funakoshi, J. Appl. Phys. 64 (3) (1988) 1000.
[26] A. Brown, B. Lewis, J. Phys. Chem. Solids 23 (1962) 1597.
[27] A. Stegherr, Ph.D. Thesis, Aachen, 1969.
[28] A. Stegherr, Philips Res. Reports. 6 (1969) 1.
[29] Natl. Bur. Stand. (U.S.) Monogr. 25 (3) (1969) 8.
[30] V.D. Das, N. Soundararajan, J. Appl. Phys. 65 (6) (1989) 2332.
[31] C.M. Garner, L.R. Gilbert, C. Wood, J. Non-Cryst. Solids 15 (1974) 63.
[32] G.B. Reddy, A. Dhar, L.K. Malhotra, E.K. Sharmila, Thin Solid Films 220 (1992) 111.
[33] A. Mzerd, D. Sayah, J.C. Tedenac, A. Boyer, Phys. Status Solidi A 141 (1994) 183.
[34] T.C. Patel, P.G. Patel, Mater. Lett. 3 (1–2) (1984) 46.
[35] E. Hatta, J. Nagao, K. Mukasa, Z. Phys. B 98 (1995) 33.
[36] G.I. Makovetski, G.M. Shakhlevich, Inorg. Mater. 18 (2) (1982) 186.
[37] I. Barin, Thermodynamic Data of Pure Substances, 2nd Edition, Weinheim, 1992.
[38] I. Barin, O. Knacke, O. Kubaschewski, Thermodynamic Properties of Inorganic Substances, Berlin, 1977.
[39] I.F. Kononyuk, V.V. Vashuk, A.S. Layashevich, Inorg. Mater. 14 (1978) 1.
[40] E. Uchida, H. Kondoh, J. Phys. Soc. Jpn. 11 (1) (1956) 21.
[41] E. Westrum, J. Machol, R. Machol, J. Chem. Phys. 29 (4) (1958) 824.
[42] M. Ettenberg, K. Komarek, E. Miller, J. Solid State Chem. 1 (1970) 583.
[43] K. Klepp, K. Komarek, Monatsh. Chem. 103 (1972) 934.

[44] A. Kjekshus, K.P. Walseth, Acta Chem. Scand. 23 (1969) 2621.
[45] K. Schubert, W. Burkhardt, P. Esslinger, E. Günzel, H.G. Meissner, W. Schütt, J. Wegst, M. Wilkens, Naturwissenschaften 43 (11) (1956) 248.
[46] A. Kjekshus, T. Rakke, A.F. Andresen, Acta Chem. Scand. A 28 (9) (1974) 996.
[47] S. Heinrich, H.U. Rexer, K. Schubert, J. Less Com. Met. 60 (1978) 65.
[48] M.B. Vellinger, R. DeJonge, C.U. Haas, Solid State Chem. 2 (1970) 299.
[49] O. Knop, R.D. McDonald, Can. J. Chem. 39 (1961) 897.
[50] A.A. Yanaki, V.A. Obolonchik, Inorg. Mater. 9 (12) (1973) 1855.
[51] H. Boller, H. Nowotny, Monatsh. Chem. 95 (1964) 1272.
[52] P. Jensen, A. Kjekshus, T. Skansen, Acta Chem. Scand. 20 (1966) 403.
[53] A.T. Dinsdale, SGTE data for pure elements, Calphad 15 (1991) 317.
[54] T.B. Massalski (Ed.), Binary Alloy Phase Diagrams, 2nd Edition, Ohio, 1990.
[55] Pearson's Handbook of Crystallographic Data, Vol. 4, 1st Edition, Materials Park Ohio, 1991.
[56] JANAF Thermochemical Tables, 3rd Edition, New York, 1986.
[57] K.C. Mills, Thermodynamic Data for Inorganic Sulphides, Selenides, Tellurides, London, 1974.
[58] Gmelin Handbook Ni Suppl. Vol. B2, 8th Edition, Weinheim, 1966.
[59] Gmelin Handbook Mo Suppl. Vol. B9, 8th Edition, Berlin, 1994.
[60] K.D. Dobson, I. Visoly Fischer, G. Hodes, D. Cahen, Sol. Energy Mater. Sol. Cells 62 (2000) 295.
[61] A. Niemegeers, M. Burgelman, J. Appl. Phys. 81 (1997) 2881.
[62] J. Beier, A.E. Abken, K. Durose, unpublished results.
[63] P.V. Meyers, S. Asher, M.M. Al-Jassim, in: D. Ginley, A. Catalano, H.W. Schock, C. Eberspacher, T.M. Peterson, T. Wada (Eds.), Proceedings of the Symposium on Thin Films Photovoltaic Related Devices—MRS Spring Meeting, San Francisco, 1996, p. 317.
[64] R. Glang, J.G. Kren, W.J. Patrick, J. Electrochem. Soc. 110 (5) (1963) 407.
[65] J. Gu, T. Kitahara, K. Kawakami, T. Sakaguchi, J. Appl. Phys. 46 (1975) 1184.
[66] P. Höschl, S. Kubalkova, Czech. J. Phys. B 22 (1972) 530.
[67] I. Lyubomirsky, V. Lyahovittskaya, R. Triboulet, D. Cahen, J. Electron. Mater. 26 (1997) 97.